A MULTISCALE COHESIVE LAW FOR CARBON FIBER NETWORKS

W. SCHILL [1,2,*] , L. J. ABBOTT[3], J. B. HASKINS[3]

Abstract. Better predictive models of mechanical failure in low-weight heat shield composites would aid material certification for missions with aggressive atmospheric entry conditions. Here, we develop such a model for the rapid engineering analysis of the failure limits of phenolic impregnated carbon ablator (PICA) - a leading heat shield material whose structural component is a carbon fiber network. We hypothesize inelastic deformation failure mechanisms and model their behavior using molecular dynamics simulations to calculate the binding energy. We then upscale this binding energy to the macroscale using a renormalization argument. The approach delivers insightful and reasonably accurate macroscale predictions that compare favorably to experiments. In application, the model is validated for a particular variety of PICA by comparison to experiment and would then be used to study design scenarios in different entry conditions.

[1] Lawrence Livermore National Laboratory, 7000 East Ave, Livermore, CA 94550 [2]Division of Engineering and Applied Science, California Institute of Technology, 1200 E. California Blvd., Pasadena, CA 91125. [3]Thermal Protection Materials Branch, NASA Ames Research Center, Moffett Field, CA 94035.
E-mail address: schill1@llnl.gov,lauren.j.abbott@nasa.gov,justin.b.haskins@nasa.gov.
*Corresponding author. Tel: 209 628-8874. E-mail schill1@llnl.gov (William Schill)

1. Introduction

Phenolic impregnated carbon ablator (PICA) is a leading heat shield material for thermal protection of spacecraft during atmospheric entry. Within the space community, there has been growing interest in the performance of heat shields during re-entry after extended operations in space. Mars Sample Return [1] serves as a prominent example. Additionally, concern has increased regarding the rapidly growing population of space debris in near earth orbit and corresponding increased probability of an impacted mission asset. Within the theater of re-entry and descent, these two issues motivate a critical question: If an impact event occurs, will the re-entry be able to proceed with a high confidence of success? To provide an answer to this question in specific entry scenarios, we must be able to characterize the *mechanical failure processes* of the heat shield material.

The mechanical behavior of PICA arises from its microstructure. At the micro-scale, PICA is composed of a carbon fiber network (CFN), specifically the commercially available FiberForm material. Fig. 1 illustrates the complicated structure of a CFN. The CFN is impregnated with low density phenolic to obtain PICA. During re-entry, the thermal loads pyrolyze the phenolic which out-gasses and cools the material dramatically, providing thermal protection. Modeling mechanical failure in many conventional materials—e.g. metals or glasses—is well characterized and may be understood from the viewpoint of defect mechanics (c.f. for instance [2, 3]). However, it is not immediately clear how to

apply such standard techniques to model PICA due to its highly irregular structure. The derivation of pertinent physical models for such disordered carbon fiber structure merits a specialized treatment.

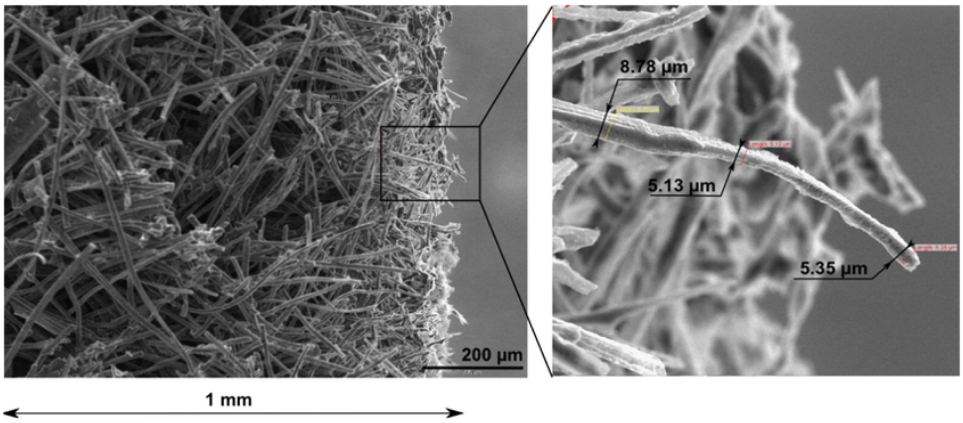

FIGURE 1. An image of the CFN of FiberForm, used for fabrication of PICA.[1]

Previous studies have been performed to understand the deterioration of PICA heat shields under typical mission operating conditions. Lachaud et al. [4] proposed a reaction-diffusion type equation to model the ablation of phenolic within the CFN matrix (see also [5]). Martin et al. [6] applied a simplified model of spall particle ejecta formation to probe the effects of carbonaceous ejecta in the flow around a reentry body. Agrawal et al. [7] performed fracture tests on notched and un-notched samples and observed a complicated response of the fibers as the notch elongated until sample failure.

More generally, CFN (or similar fiber and yarn networks) have been studied both experimentally and numerically [8, 9, 10, 11, 12, 13]. These studies invariably proceed by constructing a high fidelity finite

[1]Private communication regarding engineering and mission usages and characterization of PICA, Margaret Stackpoole, 2019

element model of a particular configuration of CFN and comparing it to a nicely constructed experiment. Long et al. [14] specializes to finite element beam models which is in principle more efficient and Zhang et al. [15] studied homogenization of representative volume elements of fiber networks. From a bottom-up modeling perspective, peridynamics modeling of CFN [16, 17] reproduced qualitatively striking aspects of fracture but ultimately were limited to relatively small simulation sizes. All these studies constitute an intriguing collection of behaviors and interrelationships of physical processes in detailed albeit highly specific test cases. However, generic insight into the energetics governing the failure of CFN material remains elusive.

To our knowledge, no model yet exists that quantitatively characterizes mechanical failure of PICA and explicitly explains this failure as a direct consequence of its microstructure.

In this paper, our goal is to provide such a model by

- identifying the mechanism by which PICA fails – i.e. forms new surfaces in response to mechanical load and
- deriving simple yet effective physical models from our understanding of these mechanisms which may be used for design.

We now outline our assumptions and strategy for accomplishing this task. Since PICA is a composite material, in principle its failure depends on both the CFN as well as the phenolic. However, order of magnitude estimates from [7, 18] suggest that the CFN is substantially stronger. We follow this assumption here and later show the network structure plays a critical role and that any effects of phenolic may be

accounted for a posteriori. In a CFN, fibers are fused together by disordered carbon interfaces which have a length scale of several microns[1]. We call these disordered carbon interfaces *joints*. We further assume the joints are composed of vitreous amorphous carbon (also known as isotropic carbon) with atomic networks resembling a three dimensional random network [19]. Previous studies have probed different amorphous carbon-carbon compounds and observed varied mechanical and thermal response, see [19] and references therein for a general overview. The observations suggest isotropic carbon fails by brittle conchoidal fracture [19]. Since individual carbon fibers possess extremely large mechanical strength, the joints are the weakest points in the CFN. Thus, the properties of the joint material in a CFN govern failure.

Under these assumptions, a natural strategy is to use lower scale principled physics simulation such as molecular dynamics to probe the inelastic strength behavior of amorphous carbon. Molecular dynamics simulations of inelastic failure [20, 21] illustrate a wide variation in strength behavior as a function of the initial amorphous carbon state and motivate the need for additional simulation studies of amorphous carbon. Thus, we perform molecular dynamics simulations of amorphous carbon under tensile loading using a configuration specifically motivated by the manufacturing process used for FiberForm.

We wish to derive a macroscale law directly from this microscale description of the amorphous carbon behavior. From general fracture mechanics theory, we conjecture that this law should have the form of a point-wise relation between a stress-like variable and a strain-like

variable across the plane of failure [3]. A formula of this type is known as a *cohesive law*. For an overview of cohesive laws, see the review article [22], which provides many different possible functional forms and references to applications for different materials. The unifying characteristic feature of a cohesive law is its non-monotonicity. The stress first increases as a function of strain and then decreases.

Many orders of magnitude separate the length scales of the bulk CFN material and the joints. Across these different length scales, it is possible that not only the action of a single joint is important, but also the combined interaction of all the joints. We adapt a theory, initially developed in the context of separation of atomic planes [23, 24] to our present context. This strategy enables us to predict the behavior of a large, but finite, number of interacting joints and link the results from molecular dynamics to the macroscale.

The specific details of this strategy result in an explicit dependence on the number of interacting joints. However, it is non-trivial in a CFN to compute a reasonable estimate of this value. To accomplish this task, we explicitly construct a representation of a carbon fiber network given a known length of each fiber, number of fibers, and relative density (i.e. the ratio of density of the bulk CFN to the density of the constituent amorphous carbon). We then use graph-theoretic methods to compute shortest traversal paths and take this as an estimate of the number of interacting fibers.

The remainder of this paper is organized into a methods section – detailing the specifics of the cohesive law derivation, molecular dynamics, and graph techniques – and a results section – wherein we show the results of the molecular dynamics calculations, the macroscale cohesive law, and compare the results to experiments.

2. Methods

In this section, we describe the methods utilized in three subsections where we

- derive a generic cohesive law as a function of the inter-fiber binding energy,
- perform molecular dynamics calculations to compute the binding energy, and
- develop a graph-theoretical approach to estimate the density of inter-fiber joints as a function of microscale parameters.

2.1. **A renormalization approach for cohesive laws.**

We begin by idealizing CFN as a 1-D chain with N joints connecting each fiber to its neighbors. This is illustrated in Fig. 2. We suppose that each fiber-fiber interaction is characterized by an *inter-fiber binding law* which relates the traction on the joint, t, to the displacement of the joint, δ. We suppose that this relationship derives from a potential, i.e.

$$t = \frac{\partial \phi}{\partial \delta} \ .$$

Furthermore, suppose that the qualitative behavior is given as in Fig. 3 such that the functional relationship possesses an inflection point at δ_c.

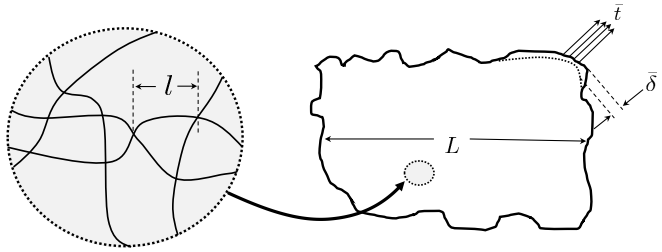

FIGURE 2. Simple idealization of CFN microstructure with inter-joint length scale l. Macroscale CFN sample with length scale L. $\bar{t}$ and $\bar{\delta}$ are a macroscale traction and displacement respectively.

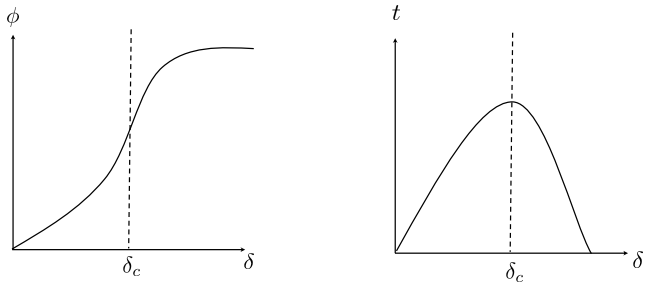

FIGURE 3. The idealized inter-fiber binding law energy and corresponding force as a function of displacement δ. A critical displacement δ_c marks the transition from increasing to decreasing traction.

We are interested in the up-scaling of such microscale knowledge to the large scale behavior of CFN of length scale $L = Nl$, see Fig. 2.

We now consider applied traction $\bar{t}$ and displacement $\bar{\delta}$ at the macroscale and endeavor to determine their relationship based on microscale physics of CFN. The following argument is due in large part to [23].

Consider the total energy of all fibers

$$E^{\text{tot}} = \sum_{i=1}^{N} \phi(\delta_i) \ . \tag{1}$$

Assuming that minimum potential energy is an appropriate governing principle, we define the macro-binding potential as

$$\bar{\phi}(\bar{\delta}) = \inf_{\{\delta_1,\ldots,\delta_N\}} \sum_{i=1}^{N} \phi(\delta_i) \ , \tag{2}$$

subject to $\bar{\delta} = \sum_{i=1}^{N} \delta_i$ and from equilibrium $t(\delta_i) = \bar{t}(\bar{\delta}) = \bar{\phi}'(\bar{\delta})$. For fixed traction t, due to the increasing-decreasing behavior of $t(\delta)$ (see Fig. 3), it is sufficient to simply consider two possible δ values. Hence, equation (2) reduces to

$$\bar{\phi}(\bar{\delta}) = \inf_{\{\delta_1,\delta_2,N_1,N_2\}} \left(N_1\phi(\delta_1) + N_2\phi(\delta_2)\right) \ , \tag{3}$$

with $N_1 + N_2 = N$ and $N_1\delta_1 + N_2\delta_2 = \bar{\delta}$. We now proceed by cases to find minimizing N_1, N_2. Consider first $N_2 = 0$ and $N_1 = N$. Then for fixed $\bar{\delta}$ as N becomes large $\delta_1 = \bar{\delta}/N$ becomes small. Hence, elastic deformation will dominate since the stiffness of the binding potential is $C = \phi''$, we obtain

$$\bar{\phi}(\bar{\delta}) = \frac{\bar{C}}{2}\bar{\delta}^2 \ ,$$

where $\bar{C} = C/N$. Second, consider the case $N_2 = 1$ and $N_1 = N - 1$. By identical argument δ_1 must be small as N becomes large for fixed δ. Consequently $\bar{\delta} \approx \delta_2$ as N becomes large. Thus

$$\bar{\phi}(\bar{\delta}) = \xi \ ,$$

where $\xi \in \mathbb{R}^+$ characterizes the large δ asymptote of ϕ. (Note, in this case, $\delta_1 \to 0$ which results in no elastic contribution.) For $N_2 > 1$, it is simple to show that the energy is larger than for the case $N_2 = 1$, so it sufficient to only consider these first two cases. Equation (3) reduces to

$$\bar{\phi}(\bar{\delta}) = \min\left(\frac{\bar{C}}{2}\bar{\delta}^2, \xi\right) , \tag{4}$$

which leads to the transition condition at $\delta = \delta_c$

$$\frac{\bar{C}}{2}\bar{\delta}^2 = \xi ,$$

which is then solved for

$$\delta_c = \sqrt{\frac{2N\xi}{C}} .$$

Inserting this into the expression for $\bar{\phi}'(\bar{\delta})$ we obtain

$$\sigma_c = \bar{t}(\delta_c) = \sqrt{\frac{2C\xi}{N}} ,$$

a macroscopic observed stress which is a decreasing function of N. If we consider a chain of N fibers each with length l, then the total length of the interacting fibers is $L = Nl$. The uniaxial critical strain follows as

$$\epsilon_c = \frac{\delta_c}{L} = \frac{\delta_c}{Nl} = \sqrt{\frac{2\xi}{NCl^2}} .$$

Finally, to relate the macroscopic stress to the microscopic stress, the ratio of the surface area of the macroscopic structure exposed to a load to that of the surface area of the load bearing components or fibers must be taken into account. Define a macro stress, σ_m, due to some loading

condition over a CFN sample over a surface area A. Furthermore, suppose that the minimal load bearing area, a, is that of the inter-fiber joints in a particular cross section of the material. Then, we have

$$\sigma_m = \frac{a}{A}\sigma_c = \frac{a}{A}\sqrt{\frac{2C\xi}{N}} \ . \tag{5}$$

We note that the factor $a/(A\sqrt{N})$ provides an a priori estimate of the change in order of magnitude between the macroscopic state of stress and that experienced at a microscopic material point.

The specific form of the cohesive potential, ϕ, will be selected and its parameters fit to results from molecular dynamics calculations. Then, the number of joints N and the ratio a/A will be computed using the graph based model.

2.2. **Molecular dynamics.** We now consider the tensile behavior of isotropic carbon and estimate the stresses involved in the formation of new surfaces. To produce an appropriate molecular dynamics model, we borrow ideas from the manufacturing process of a specific CFN material, FiberForm. In this process, phenolic is used as part of the initial mixture with carbon fibers. This mixture is then heated until all non-carbon constituents of phenolic evaporate. The remaining carbon collects in a disordered state forming the joints that connect each fiber to its neighbors. To best emulate this process, the amorphous carbon structure we use in our molecular dynamics calculations is obtained by a melt-quench procedure from a phenolic initial state.

We utilize the phenolic structure [18] pictured in Fig. 4 as the starting point for computation of isotropic carbon. We remove the hydrogen and oxygen atoms and perform an energy minimization to relax the structure. There are $13,392$ carbon atoms remaining in the simulation. We use a well-documented and validated potential for carbon-carbon interactions, ReaxFF [25], as implemented in LAMMPS [26]. In particular, ReaxFF is constructed with attention to the potential energy contributions of various chemical interactions. For a detailed discussion of an efficient implementation of this potential and its validation see [27].

We relax the structure for 0.15 ns at 3000 K using the canonical ensemble (NVT). The point here is not to fully melt the structure but allow the carbon compound to adopt a more stable configuration. The structure is then cooled to 300 K for 5700 fs. Such a cooling rate is fast but has been used before in the study of amorphous carbon structures so we take it as a reasonable point of departure [20]. In our MD calculations, the density obtained from the phenolic is $\rho \approx 1.2$ g/cm^3. We remark that we compared the calculations reported herein to those based on a dense amorphous carbon. The density of the initial carbon structure was important to get reasonable mechanical properties and detailed exploration, though beyond the present scope, would be valuable.

We then utilize a time-step of 0.5 fs to advance a molecular dynamics calculation in the isobaric-isothermal ensemble (NPT). Tensile deformation is enforced by an affine deformation of the simulation box every

10,000 time steps, while the dimensions of the box in directions normal to the deformation are allowed to relax according to maintain an isobaric system. The resulting effective strain rate is $\mathcal{O}\left(10^8 \frac{1}{s}\right)$ which is typical of molecular dynamics.

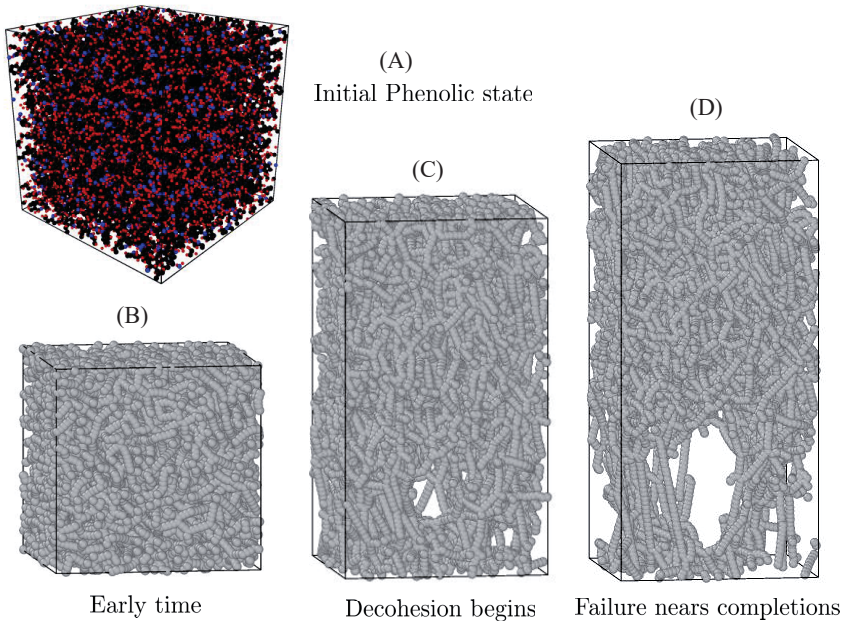

FIGURE 4. Molecular dynamics simulation cells used for mechanical property characterization. (A) Hydrogen and oxygen is systematically removed from the initial phenolic state to create a "carbonized" phenolic. The cohesive properties of the carbon material are determined through large deformations in (B), (C), and (D).

2.3. **A graph based approach to modeling carbon fiber networks.** We now develop a simple method to estimate the number of active joints in a sample of CFN material. For the calculations in this work, we adopt estimates of parameters for the FiberForm constituent of PICA following Ref. [28]. We assume a uniform distribution of fibers in both the position of their centroid and the angle relative to the

macroscopic sample. The *chop length* refers to the length of each individual fiber. We assume this to be on the order of magnitude of 1 mm. Additionally, we assume that the radius of the fiber is 10 μm. We study a representative volume element (RVE) with a side length of 1 cm. We assume an interaction length (the sample size) of 36 cm basing this on the approximate length of FiberForm and PICA coupons for tensile tests. We then populate the RVE with fibers and determine the minimal number of joints required to traverse from one side of the RVE to the other and postulate that this is a good estimate of the number of interacting joints. Further, we compute the total number of vertices which can be used to compute the ratio a/A. We compute these using Algorithm 1.

Result: Distribution of path lengths to traverse PICA sample

Require: Number of fibers, chop length, fiber angle distribution;

Generate fibers by sampling from distribution;

Compute all intersections using sweep line algorithm;

Generate graph with fiber intersections as nodes;

for *Number of fibers* **do**

  Order intersections by nearest neighbors;

  for *Number of intersections on fiber minus one* **do**

    Add an edge to graph between each intersection and its next nearest neighbor;

  end

end

Identify top and bottom nodes ;

Sample from top and bottom nodes and compute shortest path length using a breadth first search for unweighted graphs;

Algorithm 1: PICA graph model algorithm

We plot an example configuration of the CFN associated with FiberForm and PICA (in red) and the corresponding theoretical connectivity graph (in blue) generated from it by Algorithm 1 in Fig. 5. Evidently both the graph and the real space configurational representation of CFN exhibit random variations consistent with observations of samples of PICA in experiments [7]. We note that CFN can posses directional dependency (e.g orthotropic symmetry) in which case the same technique would be applicable but would require a specific treatment of the enforced symmetry.

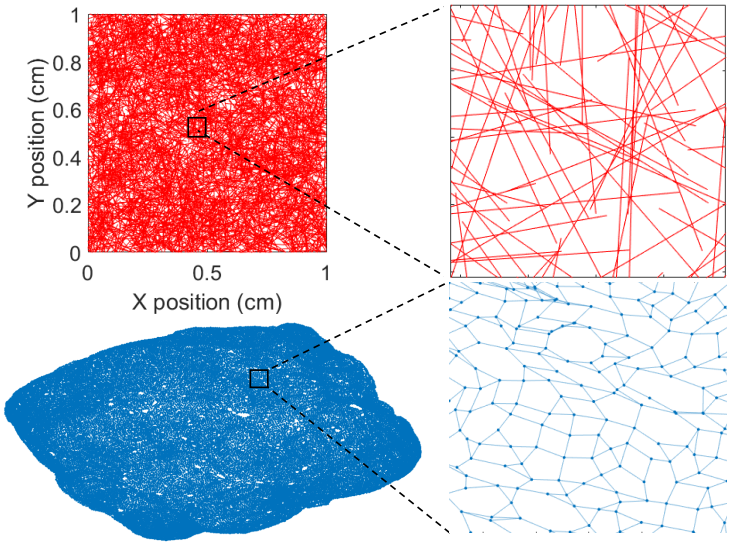

FIGURE 5. A representative volume element of the carbon fiber network. The corresponding connectivity graph representing fibers intersections as nodes.

3. Results and Discussion

We show the results of the MD calculations, the graphical model, and compare the results of the cohesive law to experiments.

3.1. **Stress strain response.** From molecular dynamics simulations, we compute several different tensile extension tests of the amorphous carbon that bond joints at different pressures and temperatures and display the results in Fig. 6. The generic behavior is consistent across all cases computed, including the characteristic lack of growth at large strains which results as a crack forms. Some of the variation in behavior, however, is less obvious. At low pressure, increasing the temperature decreases the maximum tensile strength slightly. If the carbon is preconsolidated to a high pressure, then the maximum tensile

strength increases. If the temperature is raised and then the carbon is preconsolidated, the maximum tensile strength increases by an even larger margin. This occurs because the higher temperature aids consolidation processes by increasing the kinetic rates governing atomic rearrangement. Thus, the resulting solid is a more energetically stable and consequently more difficult to break.

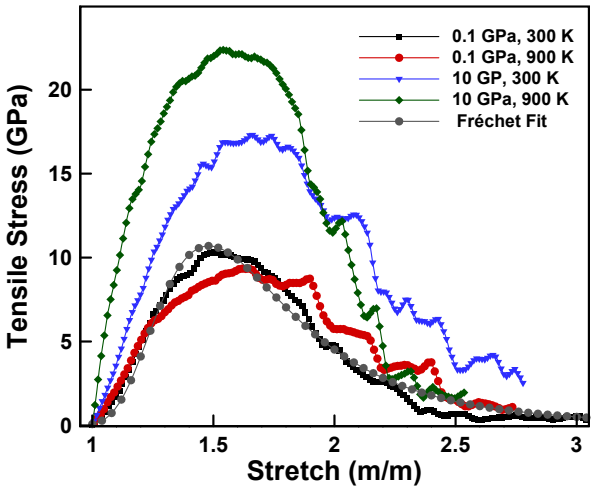

FIGURE 6. Deformation response of PICA to tensile loading at $T = 300,\ 900$ K, and $P = 0.1,\ 10$ GPa, as well as the goodness of fit of the Fréchet function to the MD data at 300 K and 0.1 GPa.

There are many possible choices for a cohesive zone law. Many examples are given in [29] and the references therein. For specificity, we adopt the Fréchet function

$$\sigma(\varepsilon) = \sigma_0 \varepsilon^{-\alpha-1} \exp\left(-\left(\frac{\varepsilon}{\beta}\right)^{-\alpha} \right) ,$$

with free parameters σ_0, α and β. We fit the free parameters to the 300 K and 0.1 GPa curve, display the parameters in Table 1, and show goodness of fit in Fig. 6. Fitting to the other curves does not alter the qualitative behavior and primarily only affects the parameter σ_0. Thus, the effect of temperature and pressure may be easily incorporated by choosing σ_0 to be some function of pressure and temperature. For instance, a power law model

$$\sigma_0 \sim T^{-\nu} p^q \ ,$$

would be a reasonable model in many instances with power law exponents, $\nu,\ q > 0$. We emphasize that the qualitative increasing-decreasing behavior is the same under all conditions examined. Thus, we expect the generic mechanisms governing the relation to the macroscale to be consistent independent of pressure and temperature. Consequently, for simplicity of discussion, we will proceed with the constants listed in Table 1.

TABLE 1. Parameter values for the Fréchet fit to MD data of tensile failure of carbonized phenolic.

σ_0	α	β
8.82929 GPa	4.96268	1.53662

3.2. **Scaling of the fiber network.** The minimum number of joints needed to traverse a CFN sample is determined by the calculation described in Algorithm 1. Depending on the beginning and ending joints located on opposite sides of the RVE, there is a distribution of various minimal path lengths. The input parameters given in Alg. 1 are

kept constant, however the resulting distribution is a function of the random initialization of the fiber locations and angles. In Fig. 7, three histograms resulting from different initializations are shown. There is relatively little variation in average and standard deviation between different random initializations of the fiber network. This suggests that the subsequent analysis is robust with respect to the fiber distribution. Thus, we note the mean of the distribution is about ~ 240 and we utilize this value hereafter in calculations.

Thus, we assume that the average number of joints across the volume is well represented by the above computation. For the assumptions of the model discussed subsequently, we take the total number of fibers to be $N \sim$ *number of joints across the RVE*$\times$*number of RVEs across one coupon* ~ 9000.

Finally, we estimate the fraction of load bearing material by

$$\begin{aligned}\frac{a}{A} &\sim \textit{number of joints in cross section} \times \textit{area of single joint} \\ &\sim 63966 \times (5 \times 10^{-4})^2 \sim 0.01 \ ,\end{aligned}$$

where we have utilized the configuration specified in Fig. 5 (noting that the total cross sectional area is 1 cm^2) and estimated the size of the cross sectional area of a single joint by examining Fig. 1 to be the projected contact area between two fibers $\approx 25\mu m$.

Thus, the parameters of the theory depend on density and follow the scaling suggested by Fig. 8 (A) and (C) (the trend lines are denoted in green)

$$\frac{a}{A} \sim \rho^2 \ ,$$

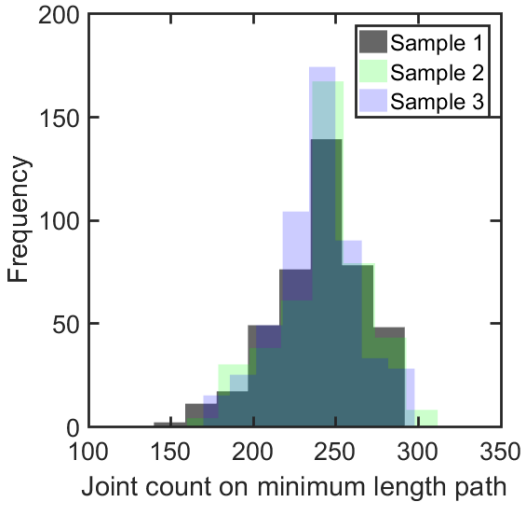

FIGURE 7. Distributions of the minimum number of fiber joints to traverse the RVE along a path. A comparison of three distributions is made using different random initial conditions to construct the RVE. The mean and standard deviation are consistent across all cases tested. The initial conditions generate different histograms and bound the statistics of the graph model.

and

$$N \sim \rho \ .$$

From Fig. 8, (B) and (D), we see that the number of vertices increases with the chop length and the total number of fibers.

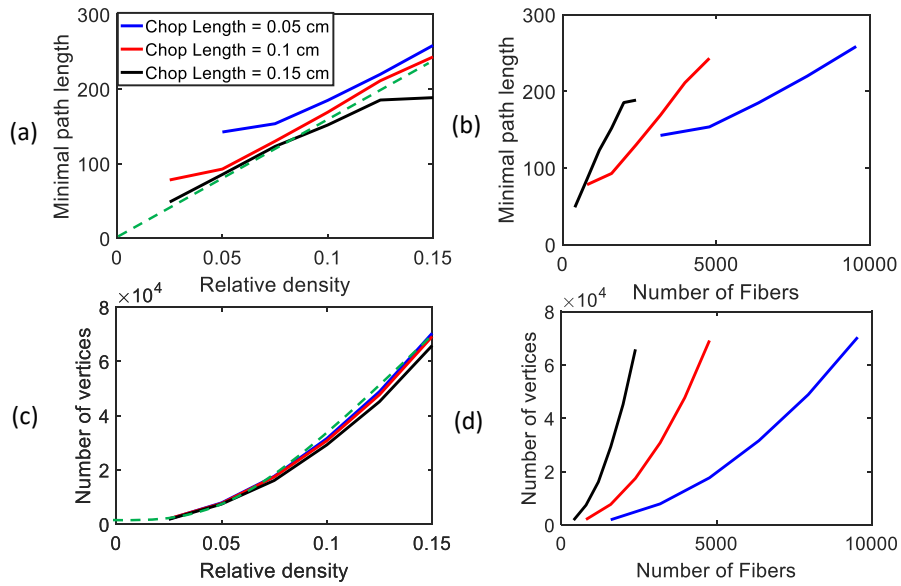

FIGURE 8. The dependence of the number of active joints and the total number of joints on the density and the number of fibers as well as the relationship to chop length. All lengths are in cm.

3.3. **Comparison to experiment.** We now compare predictions of the model to experimental tensile tests of FiberForm supplied by the manufacturer, Fiber Materials, Inc., as well as published [7] and unpublished data from testing performed on FiberForm and PICA internally by past programs at NASA Ames Research Center.

As the properties of PICA are proprietary, the examination of fracture is performed in relative units. Consider some reference density ρ_0. Based on order of magnitude estimates from experiments[2], we assume that the number of interacting fibers at this reference density is $N \approx 9000$, and the ratio of load carrying cross sections is $a/A \approx 0.01$. The experimental densities reported are $\rho = \rho_0$, $\rho = 0.62\rho_0$, and $\rho = 0.53\rho_0$. Based on the scaling of N and a/A as a function of density

we directly compute the renormalized curves. We plot the result of this calculation in Fig. 9 (A) where the vertical axis shows stress and the horizontal axis shows strain. For comparison in Fig. 9 (A), we also plot experimental data points taken from tensile tests of PICA variant coupons. The actual experimental values plotted are strain to failure and ultimate strength. The different colors indicate the different densities of PICA variant tested. We note that there is substantial scatter in the low density experimental data (which is common in these materials [7]) and that the higher density experimental data only report one test point per density.

The best criterion for comparison is to compare the peak of each of the model curves to the data points. This is due to the fact that at macroscopic time scales, once the material reaches the peak stress, the stressed state of the material will relax extremely quickly. The peak of each of the model curves exhibits strong agreement with experimentally reported values and the correct behavior as a function of density is reproduced.

As a second mode of comparison, we examine some data collected from in-house experiments at NASA Ames on FiberForm. FiberForm has a directional dependence arising from the fibers being set down in a particular plane leading to a distinction between in-plane and through-plane mechanical response. From experiments and our graph based analysis, we estimate $a/A|_{\text{through plane}}$, $a/A|_{\text{in-plane}}$, $N_{\text{through plane}}$, and $N_{\text{in-plane}}$ reported in Table 2. The resulting comparison is displayed in Fig. 9 (B). Again, the peak of each of the model curves agrees closely

with the computed data though there is substantial scatter in the data. Thus, the apparent dependence on loading direction has a reasonable explanation in terms of the microscopic parameters, N and a/A.

These comparisons suggest that the joint-wise renormalized cohesive law based on atomistic binding energies as proposed in this study is a strong candidate model for the mechanism of failure. In particular, using information easily obtainable from engineering characterization such as number of fibers and diameter of fibers, we have predicted macroscopic failure properties including a nontrivial dependence of the failure behavior on relative density and orientation. This works because the cohesive energy of the amorphous carbon joints at the nano-scale, as computed from MD, is correctly translated to the macroscale by the renormalization based on the number of fibers.

We remark we have assumed that the mechanical properties in PICA are entirely dominated by the CFN. However, it would be very reasonable to consider the effect of phenolic in PICA. This would most reasonably enter the present model as a multiplicative pre-factor in equation (5). Alternatively, one could also envision that this contributes additional linkages in the network.

TABLE 2. Parameters for Fig. 9 (B) comparison.

$a/A\|_{\text{In plane}}$	$a/A\|_{\text{Through plane}}$	$N_{\text{In plane}}$	$N_{\text{Through plane}}$
0.019	0.00051	42300	2700

(A)

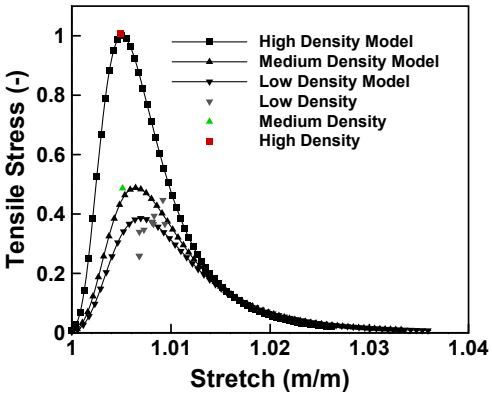

(B)

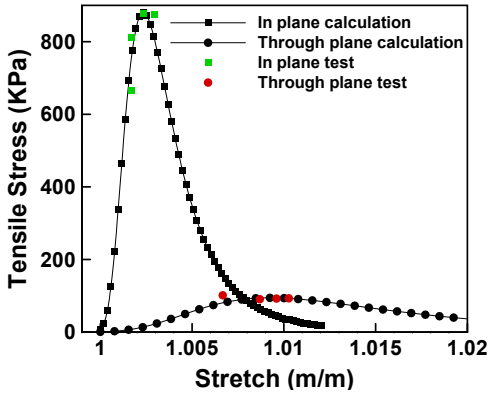

FIGURE 9. (A) Comparison of the renormalized cohesive law to several experimental measurements of PICA at 300 K. We note that as the density decreases the maximum stress decreases and the critical strain increases. The samples were measured in plane and were not charred. Note: The vertical axis has been re-scaled to fractions of the maximum observed stress. (B) Comparison of the renormalized cohesive law to several experimental values of the ultimate tensile strength of in-house samples FiberForm with different densities of random CFNs at 300 K. The maximum stress decreases and the critical strain increases in the transition from in-plane to through-plane loading.

4. Summary and Concluding Remarks

We have formulated a simple and micro-mechanically motivated model for the ultimate tensile strength of carbon fiber network materials motivated by space flight and re-entry applications of FiberForm and PICA. We have performed molecular dynamics calculations to characterize tensile failure at various pressures and temperatures. A naive comparison of molecular dynamics results to macroscopic stress measurements, without taking into account intermediate length-scales, is prone towards severe over prediction of thresholds of material failure. Our model uses arguments from renormalization theory to establish the interaction of a large, but finite, number of fibers. This accounts effectively for the disparate length-scales. Interestingly, this places CFN materials in the same universality class of cohesive behavior as cleavage of atomic planes. This provides an atomistic characterization of the material behavior and, when used in tandem with the scaling argument, delivers a prediction of the binding energy, strain, and stress at the macroscale. To account for the non-trivial consequences of dealing with a complex carbon fiber network, we utilized techniques from graph theory to derive the inputs to our model not provided by molecular dynamics, i.e. those having to do with the number of joints. We compared the results of the theory to experiments conducted in house at NASA Ames Research Center and have found good agreement.

Several lines of inquiry are immediately suggested by this study. PICA possesses a complex micro-structure which dictates its macroscale thermo-mechanical response to engineering usage. The cohesive

law can be combined with standard computational mechanics techniques – e.g. finite elements, peri-dynamics – to calculate the mechanical response of large scale systems. As discussed in the introduction, an application of high interest to the authors is to model a micrometeoroid impact event into a heat shield and assess the functionality of a thermal protection system during re-entry.

It is worth commenting on the transportability of this model to specific systems which may not share the exact numerical values assumed herein and used to compute the presented examples. Additional MD calculations are merited varying thermodynamic quantities such as the initial density which can have significant variability in a disordered solid [19]. The number of calculations needed would depend on the thermodynamic operating range of the specific application. Measurements of the application specific CFN would ideally be made estimating the chop length, number of fibers per volume, and fiber radius. From this, following Fig. 8 the parameters of the theory can be estimated.

In our opinion, further study of the nature of carbon fiber networks as it pertains to failure is also merited. The theory proposed herein is quasi-1D and thus oversimplified. The full treatment of disordered networks is a challenging question. Direct simulation is limited due to computational cost. One possible avenue to success, however, would be to introduce additional ideas from graph theory to characterize the random network to either directly compute macroscopic failure behavior or to predict micro-mechanically motivated estimates of parameters for reduced theories such as the one presented herein.

There are additional effects which could lead to softening behavior at the micro or meso-scale which we have not taken into account in this study. First, we have assumed that there is no necking at the joints. However, necking is a common pre-failure deformation process. Similarly, thermal effects where the temperature increases substantially due to plastic deformation results in a decrease in yield strength. Finally, chemical effects such as oxidation (c.f. for instance the studies [30, 31, 32]) constitute an additional contribution to the material properties and potentially results in weakening at the fiber scale. In principle, these effects could be incorporated into our current model as additional weakening, however, we leave such enhancements to future application specific work.

Acknowledgments

JBH and LJA gratefully acknowledge support through the NASA Entry Systems Modeling (ESM) project. WJS gratefully acknowledges support through the NASA Space Technology Research Fellowship. The bulk of the work contained herein was completed while WJS completed graduate studies at Caltech and has since moved to LLNL (Lawrence Livermore National Security, LLNL-JRNL-808494). We would like to thank J. Monk for interesting discussions and for providing phenolic atomistic configurations. Resources supporting this work were provided by the NASA High-End Computing (HEC) Program through the NASA Advanced Supercomputing (NAS) Division at Ames Research Center.

References

[1] Richard Mattingly and Lisa May. Mars sample return as a campaign. In *2011 Aerospace Conference*, pages 1–13. IEEE, 2011.

[2] Allan F Bower. *Applied mechanics of solids*. CRC press, 2009.

[3] Melvin F Kanninen and Carl H Popelar. *Advanced fracture mechanics*. Number 15. Oxford University Press, 1985.

[4] Jean Lachaud, Ioana Cozmuta, and Nagi N Mansour. Multiscale approach to ablation modeling of phenolic impregnated carbon ablators. *Journal of Spacecraft and Rockets*, 47(6):910–921, 2010.

[5] Joseph C Ferguson, Francesco Panerai, Jean Lachaud, and Nagi N Mansour. Theoretical study on the micro-scale oxidation of resin-infused carbon ablators. *Carbon*, 121:552–562, 2017.

[6] Alexandre Martin, Sean CC Bailey, Francesco Panerai, Raghava SC Davuluri, Huaibao Zhang, Alexander R Vazsonyi, et al. Numerical and experimental analysis of spallation phenomena. *CEAS Space Journal*, 8(4):229–236, 2016.

[7] Parul Agrawal, Jose F Chavez-Garcia, and John Pham. Fracture in phenolic impregnated carbon ablator. *Journal of Spacecraft and Rockets*, 50(4):735–741, 2013.

[8] Yao Zhang, Zixing Lu, Zhenyu Yang, Dahai Zhang, Jianjun Shi, Zeshuai Yuan, and Qiang Liu. Compression behaviors of carbon-bonded carbon fiber composites: Experimental and numerical investigations. *Carbon*, 116:398–408, 2017.

[9] Yao Zhang, Zixing Lu, Zhenyu Yang, Dahai Zhang, Junning Li, Jianjun Shi, Zeshuai Yuan, and Haikun Chen. Resilient carbon fiber network materials under cyclic compression. *Carbon*, 155:344–352, 2019.

[10] Guoquan Luo, Liping Shi, Yesheng Zhong, Lin Yang, Xiaoliang Ma, Mingwei Li, and Xiaodong He. Compressive damage of three-dimensional random fibrous ceramic materials: A meso-mechanics modeling and experimental study. *Ceramics International*, 44(13):15690–15699, 2018.

[11] Datao Li, Wenshan Yu, Wei Xia, Qinzhi Fang, and Shengping Shen. High-temperature short-range compressive responses and contact effect of ultrahigh porosity 3d random fibrous materials. *Journal of the American Ceramic Society*, 101(10):4509–4518, 2018.

[12] Liping Shi, Kecai Long, Yesheng Zhong, Guoquan Luo, Xiaoliang Ma, Mingwei Li, Xiaodong He, and Jia Yu. Compressive and shear performance of three-dimensional rigid stochastic fibrous networks: Experiment, finite element simulation, and factor analysis. *Journal of the European Ceramic Society*, 40(1):115–126, 2020.

[13] Xiaoding Wei, Matthew Ford, Rafael A Soler-Crespo, and Horacio D Espinosa. A new monte carlo model for predicting the mechanical properties of fiber yarns. *Journal of the Mechanics and Physics of Solids*, 84:325–335, 2015.

[14] Kecai Long, Liping Shi, Yesheng Zhong, Guoquan Luo, Xiaoliang Ma, Mingwei Li, Xiaodong He, and Chunlong Guan. Effects of equivalent beam element on the in-plane shear performance of 3d stochastic fibrous networks. *Ceramics International*, 45(10):12734–12741, 2019.

[15] Mang Zhang, Yuli Chen, Fu-pen Chiang, Pelagia Irene Gouma, and Lifeng Wang. Modeling the large deformation and microstructure evolution of non-woven polymer fiber networks. *Journal of Applied Mechanics*, 86(1), 2019.

[16] Florin Bobaru and Stewart A Silling. Peridynamic 3d models of nanofiber networks and carbon nanotube-reinforced composites. In *AIP Conference Proceedings*, volume 712, pages 1565–1570. American Institute of Physics, 2004.

[17] Florin Bobaru, Stewart Andrew Silling, and H Jiang. Peridynamic fracture and damage modeling of membranes and nanofiber networks. In *Proceedings of the XI International Conference on Fracture, Turin, Italy*, volume 5748, pages 1–6, 2005.

[18] Joshua D Monk, Eric W Bucholz, Tane Boghozian, Shantanu Deshpande, Jay Schieber, Charles W Bauschlicher Jr, and John W Lawson. Computational

and experimental study of phenolic resins: thermal–mechanical properties and the role of hydrogen bonding. *Macromolecules*, 48(20):7670–7680, 2015.

[19] E Savage. *Carbon-carbon composites*. Springer Science & Business Media, 2012.

[20] Ioannis N Remediakis, Maria G Fyta, Christos Mathioudakis, Georgios Kopidakis, and Pantelis C Kelires. Structure, elastic properties and strength of amorphous and nanocomposite carbon. *Diamond and Related Materials*, 16(10):1835–1840, 2007.

[21] Tian-Bao Ma, Lin-Feng Wang, Yuan-Zhong Hu, Xin Li, and Hui Wang. A shear localization mechanism for lubricity of amorphous carbon materials. *Scientific reports*, 4:3662, 2014.

[22] Kyoungsoo Park and Glaucio H Paulino. Cohesive zone models: a critical review of traction-separation relationships across fracture surfaces. *Applied Mechanics Reviews*, 64(6):060802, 2011.

[23] O Nguyen and M Ortiz. Coarse-graining and renormalization of atomistic binding relations and universal macroscopic cohesive behavior. *Journal of the Mechanics and Physics of Solids*, 50(8):1727–1741, 2002.

[24] Andrea Braides, Adrian J Lew, and Michael Ortiz. Effective cohesive behavior of layers of interatomic planes. *Archive for Rational Mechanics and Analysis*, 180(2):151–182, 2006.

[25] Kimberly Chenoweth, Adri CT Van Duin, and William A Goddard. Reaxff reactive force field for molecular dynamics simulations of hydrocarbon oxidation. *The Journal of Physical Chemistry A*, 112(5):1040–1053, 2008.

[26] Steve Plimpton. Fast parallel algorithms for short-range molecular dynamics. *Journal of Computational Physics*, 117(1):1 – 19, 1995.

[27] Hasan Metin Aktulga, Joseph C Fogarty, Sagar A Pandit, and Ananth Y Grama. Parallel reactive molecular dynamics: Numerical methods and algorithmic techniques. *Parallel Computing*, 38(4-5):245–259, 2012.

[28] Huy K Tran. Development of lightweight ceramic ablators and arc-jet test results. 1994.

[29] K Yu Volokh. Comparison between cohesive zone models. *Communications in Numerical Methods in Engineering*, 20(11):845–856, 2004.

[30] Francesco Panerai, Alexandre Martin, Nagi N Mansour, Steven A Sepka, and Jean Lachaud. Flow-tube oxidation experiments on the carbon preform of a phenolic-impregnated carbon ablator. *Journal of Thermophysics and Heat Transfer*, 28(2):181–190, 2014.

[31] Francisco Torres-Herrador, Jeremie BE Meurisse, Francesco Panerai, Julien Blondeau, Jean Lachaud, Brody K Bessire, Thierry E Magin, and Nagi N Mansour. A high heating rate pyrolysis model for the phenolic impregnated carbon ablator (pica) based on mass spectroscopy experiments. *Journal of Analytical and Applied Pyrolysis*, 141:104625, 2019.

[32] Hsi-Wu Wong, Jay Peck, James Assif, Francesco Panerai, Jean Lachaud, and Nagi N Mansour. Detailed analysis of species production from the pyrolysis of the phenolic impregnated carbon ablator. *Journal of analytical and applied pyrolysis*, 122:258–267, 2016.